

SYNCHROTRON RADIATION: FROM STORAGE RING TO A HARD X-RAY BEAMLINE

Didem KETENOGLU* 

Received: 02.03.2019 ; revised: 22.04.2019 ; accepted: 29.04.2019

Abstract: In the present study, a general overview covering the consecutive steps, starting with the release of electrons from an electron source until the generation of synchrotron radiation, is presented. A brief introduction regarding the main characteristics and fundamental components of third generation light sources as well as the radiation characteristics of different Insertion Devices are discussed. Following a concise description of a typical hard X-ray synchrotron beamline, synchrotron radiation based X-ray Raman scattering spectroscopy, which is a non-resonant inelastic hard X-ray technique, is explained. Finally, liquid water oxygen K-edge absorption spectrum recorded with a resolution of 0.8 eV at ~10 keV utilizing X-ray Raman spectrometer at PETRA III facility of DESY is presented and compared to the spectrum from the literature measured by conventional X-ray absorption spectroscopy.

Keywords: Synchrotron radiation, Storage ring, Beamline, Third generation light source, Inelastic X-ray scattering, X-ray Raman scattering spectroscopy

Sinkrotron Işınımmı: Depolama Halkasından Sert X-ışını Demet Hattına

Öz: Bu çalışmada, elektronların bir elektron kaynağından salınması ile başlayıp sinkrotron ışınımmı elde edilmesine kadarki birbirini izleyen adımları kapsayan genel bir bakış sunulmuştur. Üçüncü nesil ışınım kaynaklarının ana karakteristikleri ve temel bileşenleri ile farklı eklenti aygıtlarının ışınım karakteristikleri de tartışılmıştır. Tipik bir sert X-ışınımmı sinkrotron demet hattının kısaca tasvirinden sonra, rezonans olmayan inelastik sert X-ışınımmı tekniği olan, sinkrotron ışınımmına dayalı X-ışınımmı Raman saçılma spektroskopisi açıklanmıştır. Son olarak, DESY-PETRA III sinkrotronundaki X-ışınımmı Raman spektrometresi kullanılarak, ~10 keV enerjide 0.8 eV çözünürlükle kaydedilen sıvı fazdaki suyun oksijen K-soğurma sınırı spektrumu sunulmuş ve literatürde geleneksel X-ışınımmı soğurma spektroskopisi ile ölçülen spektrum ile karşılaştırılmıştır.

Anahtar Kelimeler: Sinkrotron ışınımmı, Depolama halkası, Demet hattı, Üçüncü nesil ışınım kaynağı, Inelastik X-ışınımmı saçılması, X-ışınımmı Raman saçılma spektroskopisi

1. INTRODUCTION

Following Röntgen's discovery of the first X-ray tube (Lindgaard-Andersen and Gerward, 1995), scientific efforts were expeditiously carried out to enhance the brilliance and quality of light sources. As the technology rapidly developed starting from the mid-20th century, light sources marked an era in terms of their radiation generation mechanisms. Therefore accelerator-based light sources came into prominence owing to their superior radiation characteristics. In contrast to traditional light sources (e.g. solid state lasers), the use of free electrons under ultra-

*Department of Physics Engineering, Faculty of Engineering, Ankara University, 06100 Tandoğan, Ankara
Corresponding Author: Didem Ketenoglu (dketen@eng.ankara.edu.tr)

high vacuum in particle accelerators enabled generation of much more brilliant and powerful radiation.

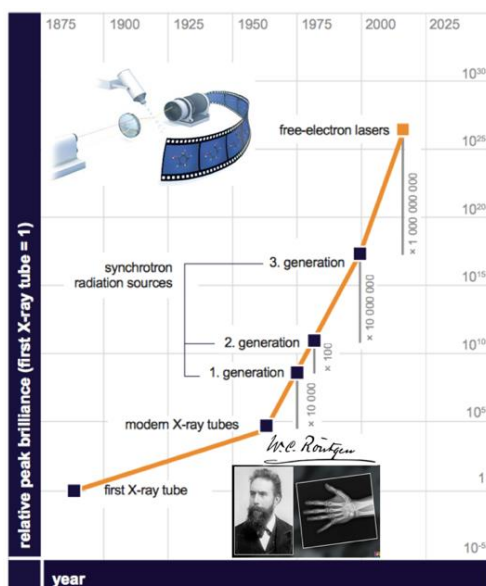


Figure 1:
Chronological evolution of light sources in terms of their peak brilliance
 <https://www.xfel.eu/news_and_events/flyers_and_brochures/index_eng.html>

In the 1960s, circular accelerators were dedicated to high energy physics experiments and nuclear research. Parasitic radiation generated by bending magnets in storage rings was called 1st generation synchrotron radiation. As synchrotron-based scientific research rapidly progressed from 1950 to 2000, the idea of using periodic magnetic structures (Insertion Devices, IDs) emerged for generation of high brilliance and high power radiation. The radiation generated by wigglers was called 2nd generation synchrotron radiation. After the developments on circular accelerators, by passing low-emittance electron bunches (i.e. ~3-25 nm.rad in horizontal direction) through undulator structures, 3rd generation synchrotron radiation was obtained. Compared to horizontal emittances of 1st and 2nd generation synchrotron machines (~100-200 nm.rad), 3rd generation sources provide ~8-33 less horizontal emittance, resulting in much more brilliant radiation. Considering the brilliance, modern synchrotron facilities provide ~10¹⁵-10²⁰ higher peak brilliance than the first X-ray tubes (Fig. 1). On the other hand, linear accelerators were utilized to achieve ultra-low-emittance beam both in vertical and horizontal directions and 4th generation light sources (called Free-Electron Lasers) provided remarkable improvement on brightness, coherence and pulse length.

2. WORKING PRINCIPLE OF A STORAGE RING

Concerning physical concepts and machine aspects, the basic principle of a synchrotron is that, the electrons traveling approximately at the speed of light c ($3 \cdot 10^8$ m/s) are forced by magnetic fields to maintain a circular trajectory. First, electrons are released from an electron source such as a thermionic DC gun or photocathode RF gun into a linear accelerator (linac) to be accelerated to some MeV energies. Then, the electrons are forwarded to a booster ring in order to increase their energy from MeV to GeV scale. Finally, the electron bunches are transferred to the main storage ring where they are maintained at a fixed energy (Fig. 2).

Circulating electrons in a storage ring lose some amount of energy at each turn as seen in Eq. 1, where e is the electron charge, R is the curvature radius and E is the electron beam energy. According to Eq. 1, increasing electron beam energy in a storage ring results in E^4 order of energy loss per turn. In order to maintain the electrons in a circular path, the energy loss has to be fully provided by accelerating RF cavities located at straight sections of storage rings. An array of different types of magnets in a storage ring such as quadrupole magnets work to maintain the electron emittance in the transverse plane and dipole magnets bend the electrons on a circular trajectory.

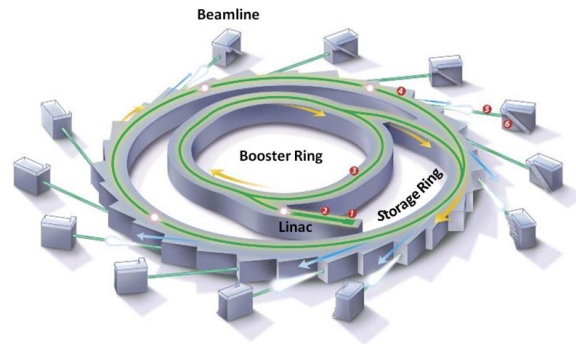


Figure 2:

Schematic view of a storage ring

<<http://archive.synchrotron.org.au/synchrotron-science/what-is-a-synchrotron>>

$$\Delta E_e = \frac{4\pi e^2}{3 R} \left[\frac{E}{mc^2} \right]^4 \quad (1)$$

One of the most important parameters of a storage ring, which directly gives the average beam current, is the time structure of electron bunches (Fig. 3). In order to achieve synchronization between electron bunches and accelerating RF field in the time domain, bunch separation has to be an integer multiple of the RF period (called harmonic number), hence the name “synchrotron” comes out. For instance, PETRA III synchrotron (Ascone et al., 2004) of Deutsches Elektronen-Synchrotron (DESY) operates at 100 mA average current with 769 nC beam charge and one can easily find the bunch separation of 7690 ns by Eq. 2 for single bunch mode. Since the operational RF frequency of PETRA III is approximately 500 MHz (2 ns RF period in time domain), the harmonic number is calculated as 3840. Finally, summarizing the time structure of PETRA III, the rms length of the electron bunches is 44 ps with a time interval of 7690 ns for single bunch mode.

$$t = \frac{Q}{I_{ave.}} \quad (2)$$

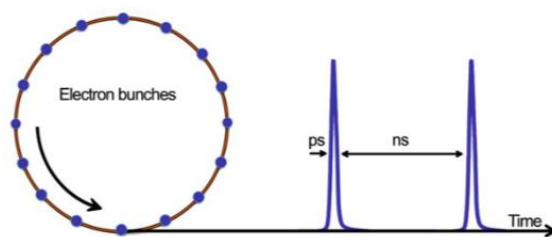


Figure 3:
Schematic time structure of electron bunches in a synchrotron
 <(Balerna and Mobilio, 2015)>

Table 1 summarizes the comparison of beam energies and circumferences of world’s leading synchrotron radiation facilities. Since the beginning of the 1990s, different synchrotron light sources have been commissioned for dedicated user experiments.

Table 1. Leading synchrotron radiation facilities around the World
 <(https://lightsources.org, https://www.slri.or.th/en/index.php/synchrotron-around-the-world.html)>

Facility	Country	Beam Energy [GeV]	Circumference [m]	Start of User Operation
ASTRID	Denmark	0.58	40	1991
ESRF	France	6	844	1992
ALS	US	1.9	196	1993
ELETTRA	Italy	2-2.4	260	1993
APS	US	7	1104	1995
SPring-8	Japan	8	1436	1997
ANKA, KIT	Germany	2.5	110	2000
SLS, PSI	Switzerland	2.8	288	2001
CLS	Canada	2.9	147	2004
Australian Synchrotron	Australia	3	216	2006
DLS	UK	3	561	2006
SOLEIL	France	3	354	2006
MAX-III	Sweden	0.7	36	2008
PETRA III, DESY	Germany	6	2304	2009
ALBA	Spain	3	270	2010
NLSLS-II	US	3	792	2015
MAX-IV	Sweden	3	528	2015
SIRIUS	Brazil	3	518	2019

3. SYNCHROTRON RADIATION CHARACTERISTICS AND INSERTION DEVICES

When radiation characteristics of light sources are compared, the concept of brilliance comes into prominence. Accelerator based 3rd generation light sources attain high peak brilliance up to 10^{25} photons/s/mrad²/mm²/0.1% BW (Fig. 4).

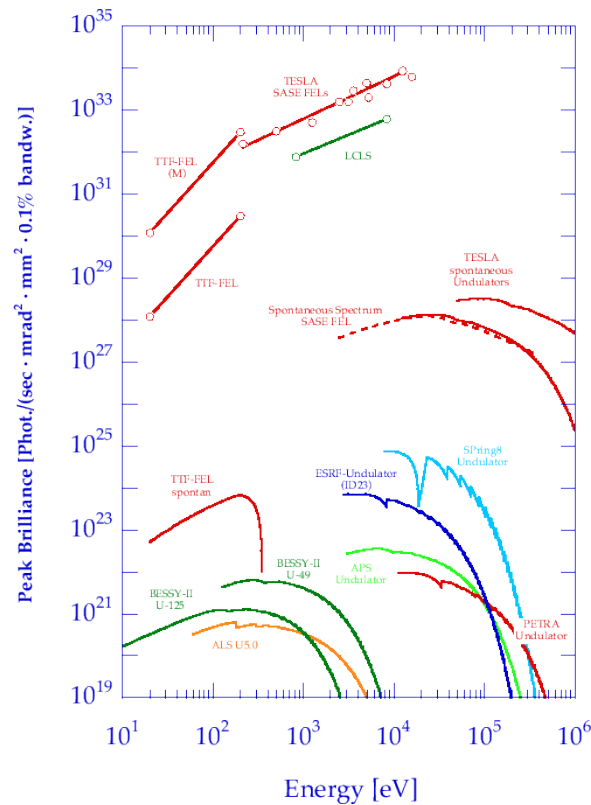


Figure 4:
Peak brilliance vs photon energies for 3rd and 4th generation light sources
<(Richard et al., 2001)>

Spectral brilliance is the number of photons per second per source area per source divergence per spectral bandwidth in units of photons/s/mm²/mrad²/0.1%BW and basically defined as photon flux divided by emittance:

$$B = \frac{n_{ph}}{\Delta t \cdot \varepsilon_x \cdot \varepsilon_y \cdot 0.1\% BW} \quad (3)$$

Concerning the correlation between brilliance and emittance, one should first start with the definition of the flux of a source:

$$\Phi = \frac{n_{ph}}{\Delta t \cdot 0.1\% BW} \quad (4)$$

where, n_{ph} is the number of photons, Δt is the unit time and BW is the bandwidth in terms of photon energy or wavelength. For instance, at 1 keV nominal photon energy, 0.1%BW denotes an energy range of 999.5 eV to 1000.5 eV. On the other hand, the size and the angular distributions of a source have great importance on its serviceability. In this respect, one can consider the intensity as a distribution, where standard deviation of this distribution is characterized by spatial extensions, σ_x and σ_y , horizontal and vertical sizes, respectively. In addition, angular distribution of the flux is defined by standard deviation of the intensity through a nominal direction, σ'_x and σ'_y , where the subscripts x and y denote the horizontal and vertical planes, respectively. As a result, the horizontal and vertical emittances of a source are described by Eqs. 5-6.

$$\varepsilon_x = \sigma_x \sigma'_x \quad (5)$$

$$\varepsilon_y = \sigma_y \sigma'_y \quad (6)$$

Additionally, synchrotron light sources provide continuous and wide spectral range from infrared to hard X-rays (Fig. 5), tunable wavelength (simply by gap change of IDs), pulsed time structure, linear or circular polarized radiation depending on ID type (i.e. planar or helical) and collimated photons.

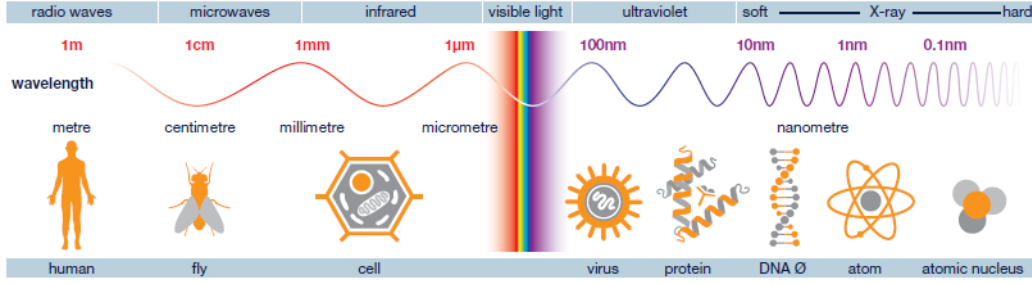


Figure 5:

The electromagnetic spectrum

<(https://www.xfel.eu/news_and_events/flyers_and_brochures/index_eng.html)>

IDs (wigglers and undulators) can be defined as an alternating sequence of dipole magnets on parallel girders (Fig. 6). When electron bunches enter the undulator line, they are compelled by periodic magnetic forces to follow a “slalom-like trajectory” on a horizontal plane, resulting in generation of high power radiation. The most important parameter of an ID is the parameter K (Eq. 7), which is directly derived from the peak magnetic field. In Eq. 8, g is the undulator gap, λ_u is the undulator period and a , b , c are the coefficients which depend on the magnetic configuration of the insertion device. Typically, when the parameter K is less than 3, magnetic field profile is approximately sinusoidal, hence the name “undulator” comes out.

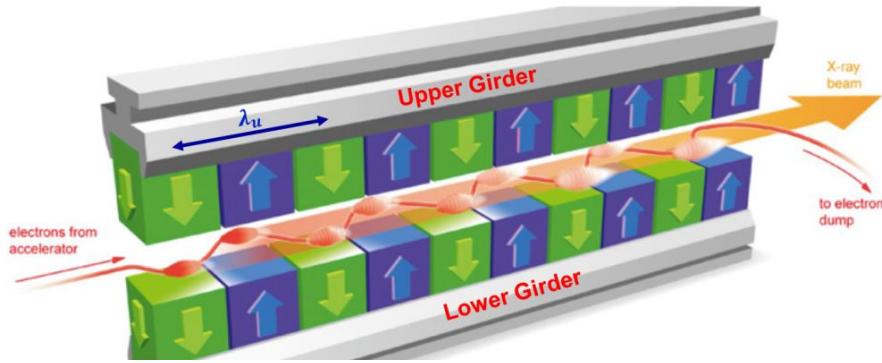


Figure 6:

Schematic view of a planar undulator

<(https://www.xfel.eu/news_and_events/flyers_and_brochures/index_eng.html)>

$$K = 0.934 \lambda_u [cm] B_{peak} [T] \quad (7)$$

$$B_{peak} = a \text{Exp} \left[b \frac{g}{\lambda_u} + c \left(\frac{g}{\lambda_u} \right)^2 \right] \quad (8)$$

For IDs, helical and planar devices are available with regard to their magnetic structures. Even though an helical undulator provides circular polarization, which is an important feature in some user experiments, the tuning process is slightly difficult due to its relatively-complicated magnetic structure. Complications in pole tuning may arise because of the fact that both horizontal and vertical components of the magnetic field are involved in helical devices. As a result, almost all accelerator-based light sources utilize planar undulators because of their less complicated nature in pole tuning process.

4. A USER EXPERIMENT AT A SYNCHROTRON BEAMLINE

After the synchrotron radiation is generated, it is transferred to experimental stations, called beamlines, which are located around the storage ring. The length of a typical beamline at a synchrotron facility is a distance of approximately 25 to 100 meters from the storage ring to the end station. Beamlines host specialized devices and equipment that are used for monochromatizing, focusing and collimating the beam. An X-ray beam is transferred through a set of equipment onto sample and data is recorded. Required characteristics (e.g. energy resolution, beamsizes etc.) of the beam illuminating the sample as well as the interaction type with matter determine the components utilized at the beamlines. Each beamline is designed for a particular field of research and beamline equipments are located in radiation shielded hutches. A beamline consists of “optics hutches”, “experimental hutches” and “control hutches”, all aligned in a row. In Fig. 7, a schematic overview of the fundamental components in a typical hard X-ray beamline is presented.

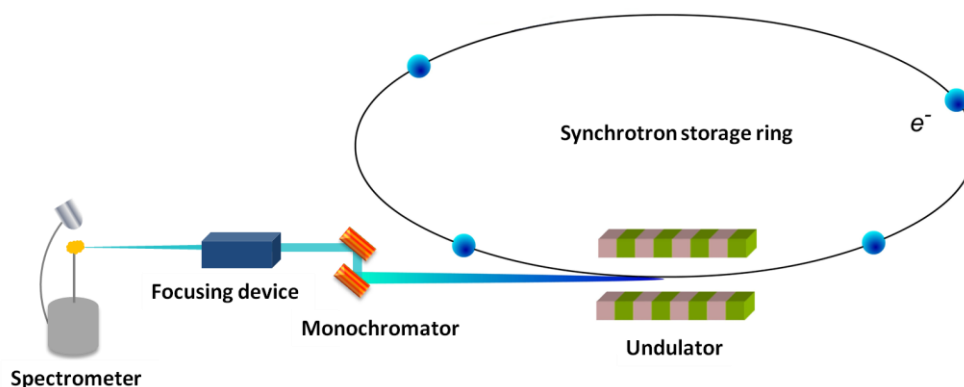


Figure 7:
Schematic overview of the fundamental components in a typical hard X-ray beamline

In an optics hutch, the undulator beam is passed through a double-crystal monochromator (DCM) which is utilized to perform the first monochromatization while taking the excessive heat load in order to protect the instruments further downstream. A double crystal monochromator includes two parallel single crystals providing a single required wavelength of radiation with a narrow bandwidth. A channel-cut crystal (high resolution monochromator, HRM) is utilized when further monochromatization is necessary. Monochromatized X-rays are collimated/focused by using specialised mirrors, lenses and etc. Slits are used to clean up the beam so that only the central cone of the undulator beam is utilized. All the optics in the beamline are designed to handle high levels of heat. In addition, between the hutches, the beam travels through vacuum maintaining transport tubes. In an experimental hutch, the sample environment/condition (e.g. temperature, pressure, magnetic field etc.) is prepared for the desired experiment and sample position is precisely adjusted with respect to the beam using

multiple motors in a dedicated instrument. Finally, detectors record the radiation interacting with the sample. In control hutch, users have the opportunity to control remotely each equipment in optics and experimental hutches, as well as adjust the beam and sample position and record the data (McCarthy et al. 2018, Gomez et al. 2018, Lutzenkirchen-Hecht et al. 2014).

The unique properties of synchrotron radiation are high brilliance over a broad and continuous spectral range, energy tunability, high coherence, controlled polarization, pulsed time structure, low emittance (small angular divergence) and high stability in terms of intensity and position; which all make it an indispensable tool in the exploration of matter. Synchrotron radiation offers a wide application area in physics, chemistry, biology, medicine, material science, environmental science, art, archeology and cultural heritage (Brown and Sturchio 2002, Moffat and Ren 1997, Iwamoto 2018, Cotte et al. 2010, Basile et al. 2010). Experiments are carried out utilizing a variety of techniques, such as spectroscopy, X-ray scattering, crystallography and tomography. Experimental techniques conducted at synchrotron beamlines can be classified under three categories; spectroscopy, scattering and imaging in which the energy, momentum and position changes of the beam are measured before and after its interaction with matter. In addition, each of these techniques can be performed within time resolution.

X-ray Raman scattering (XRS), also called as non-resonant inelastic X-ray scattering (NRIXS), is a hard X-ray scattering method which provides element-specific information regarding electronic structure. XRS is utilized to probe low energy absorption edges in different phases; such as gases, liquids, solids both crystalline and weakly ordered solids. It is an effective technique to examine the structural and electronic features of technologically relevant materials, for example rechargeable batteries or hydrogen storage devices under working conditions (Braun et al. 2015, Sahle et al. 2016), inner Earth elements under realistic conditions (Lee et al. 2014), to track chemical and biological reactions in liquid medium, to discriminate ancient and historic materials comprising organic compounds (Gueriau et al. 2017). In the XRS process, an incoming photon is scattered inelastically from a core shell electron promoting it to an unoccupied level and XRS measures the intensity of scattered X-rays as a function of energy transfer. The technique provides to monitor K-edges of life elements such as carbon and oxygen or the L- and M-edges of the 3d transition metals such as iron and cobalt (~50-1000 eV) with hard X-rays (~10 keV). Measuring low energy absorption edges poses a challenge for liquids, samples under high temperature/pressure and systems under in-situ/operando conditions, as the system requires high vacuum condition in conventional methods. XRS is well suited to study in complex sample environments without any vacuum requirement, since the incident and scattered beam are in the hard X-ray region. Thanks to these properties, the method provides an alternative way to mostly used conventional X-ray absorption spectroscopy (XAS) (Yano and Yachandra 2009). In the XAS technique, the incident beam energy is selected to be around the absorption edge, while in XRS the incoming beam energy is scanned in the vicinity of the excitation energy as the scattered beam is measured at a fixed energy. In the low momentum transfers, the resulting features are identical in both techniques, however, further information is achievable for high momentum transfers in XRS (Hämäläinen and Manninen 2001, Bergmann et al. 2002(a), Huotari et al. 2010, Sahle et al. 2015). The weak scattering cross section leads to a long measurement duration in XRS experiments, but it is overcome through advanced instruments utilizing high intense synchrotron sources.

XRS studies can be conducted only at high brilliance 3rd generation synchrotron source facilities equipped with dedicated optics and spectrometers. The XRS setup at inelastic hard X-ray scattering beamline P01 of PETRA III at DESY in Hamburg, Germany is presented in Fig. 8. In the XRS experiment, the radiation from undulator was monochromatized by DCM and then focused to a 10 (Vertical) × 20 (Horizontal) μm^2 spot by Kirkpatrick-Baez (KB) mirrors with the photon flux of $\sim 10^{13}$ photons/s. 12-spherically bent Si (660) crystals were used to energy analyze of the scattered photons and the data were gathered by APDs (Avalanche Photo

Diodes) detector. Liquid water O K-edge XRS spectrum was recorded with an overall energy resolution of 0.8 eV (FWHM) at the elastic energy of 9690 eV (Fig. 9). The x -axis of the obtained spectrum shows the transferred energy calculated by subtracting the scanned incident photon energy from the fixed spectrometer energy of 9690 eV. The spectrum was measured at low momentum transfer where the average scattering angle is 30° . This is the very first measurement performed by the XRS instrument at P01 for an experimental confirmation of O K-edge liquid water spectra.

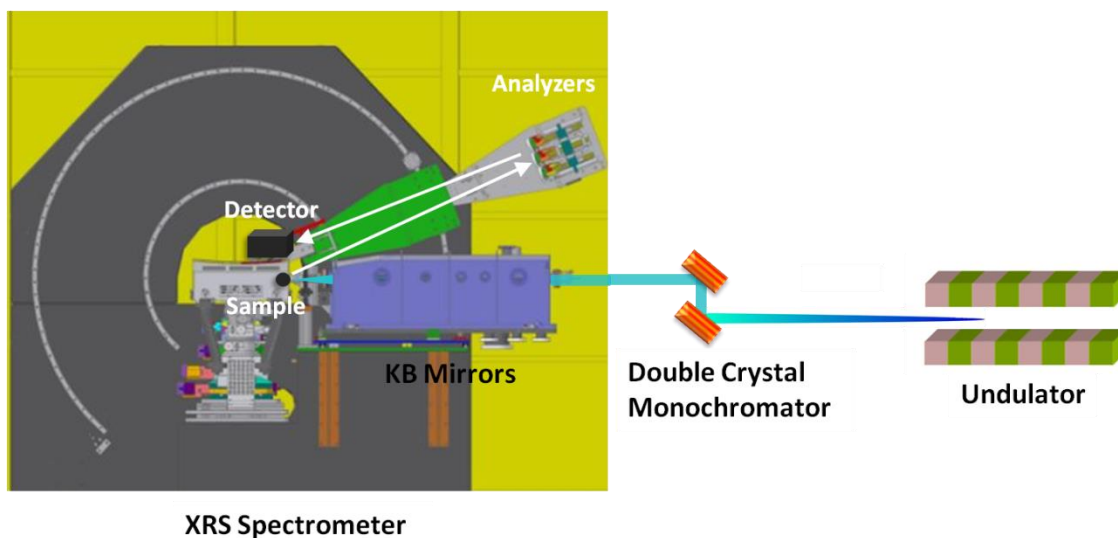


Figure 8:
Schematic setup of XRS experiment at P01 of Petra III, DESY

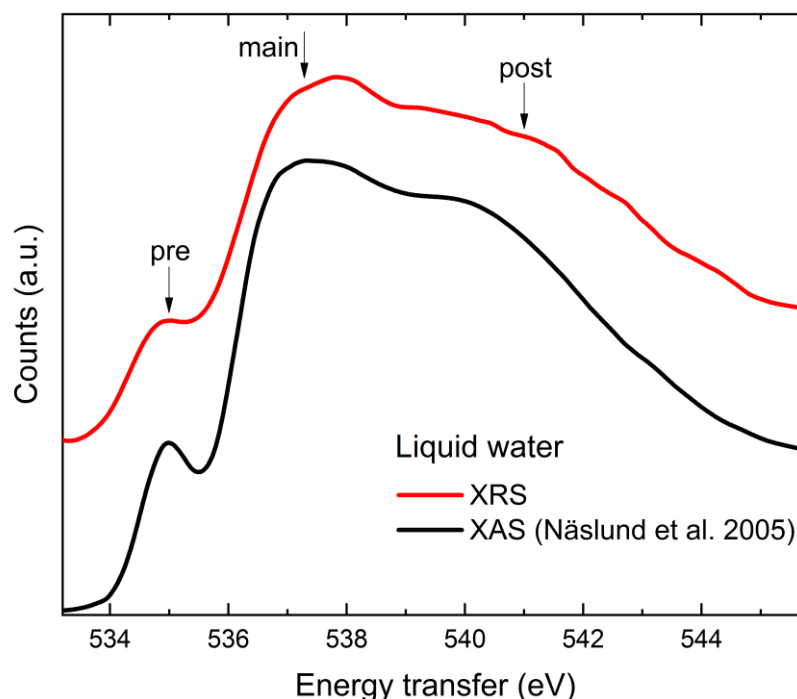


Figure 9:

The O K-edge X-ray Raman spectrum (measured) and transmission mode X-ray absorption spectrum (Näslund et al. 2005) of liquid water at room temperature

XAS and XRS have become standard techniques utilized for the study of O K-edge absorption features in different phases of water (Näslund et al. 2005, Myneni et al. 2002, Bergmann et al. 2002(b), Nilsson et al. 2010, Tse et al. 2008, Smith et al. 2006, Parent et al. 2002, Jonas et al. 2014). The conventional XAS study at oxygen K-edge of bulk water suffers from saturation effect, short penetration depth and vacuum requirement, therefore the XRS method is frequently used to determine the structure of water under extreme conditions such as high temperature and high pressure (Mao et al. 2006, Fukui et al. 2007, Iitaka et al. 2015, Cai et al. 2005, Sahle et al. 2013).

Fig. 9 presents the measured O K-edge XRS spectrum of liquid water in comparison with the transmission mode XAS spectrum by Näslund et al. 2005. The experimental resolutions are 0.8 eV for the XRS and 0.1 eV for the XAS spectra. The both spectra were collected at room temperature. XRS and XAS spectra are given as the functions of the energy transfer and the incident photon energy, respectively. The O K-edge spectra of liquid water have three regions including; a pre-edge at ~535 eV, a main-edge region at 537-538 eV and a post-edge region at 540-542 eV. The pre-edge feature stems from strongly asymmetric local configurations of the water molecules indicating that a large fraction of the molecules in liquid water exhibits strongly distorted or broken H bonds. The post-edge feature is related to strong H-bonds and results from the excitation into delocalized states in the conduction band (Tse et al. 2008, Näslund et al. 2005, Smith et al. 2006, Parent et al. 2002, Jonas et al. 2014). 10 keV X-rays used in the XRS method have access to a probing depth of mm range and besides the obtained energy resolution of 0.8 eV resolves especially the pre-peak feature. Consequently, all properties observed by XAS have reproducibility through XRS and the results exhibit the potential of the

XRS technique as a bulk sensitive probe for the investigation of liquid water without any vacuum requirement.

5. CONCLUSION

Worldwide synchrotron facilities offer high brilliance light sources and a wide range of scientific and technological applications in physics, engineering sciences, nanotechnology, geological sciences, materials science, electronics, medicine, chemistry, life sciences etc. Various measurement techniques can be performed by integrating the unique characteristics of synchrotron radiation sources with modern synchrotron beamlines which host state-of-the-art instruments. XRS is one of the hard X-ray scattering techniques that requires extremely intense radiation. The bulk-sensitive XRS technique provides the unique capability to study low energy absorption edges under extreme conditions. In addition, the use of high energy X-rays provides the penetrating power and removes the constraints of soft X-rays in the studies of complicated sample environments. The O K-edge XRS spectrum of liquid water with the resolution of 0.8 eV at the room temperature was measured at the inelastic hard X-ray scattering beamline P01 at PETRA III. Finally, the measurement demonstrated that the result agrees well with the data previously recorded through X-ray absorption spectroscopy.

ACKNOWLEDGEMENTS

The author acknowledges Manuel Harder, Georg Spiekermann, Hasan Yavaş and Hans-Christian Wille regarding the XRS experiment at beamline P01 of PETRA III, DESY.

REFERENCES

1. Ascone, I. et al. (2004) PETRA III: A Low Emittance Synchrotron Radiation Source, *Technical Design Report*, EDMS ID: D00000000822371,A,1,1
2. Balerna, A. and Mobilio, S. (2015) Introduction to synchrotron radiation, *Springer-Verlag Berlin Heidelberg*. doi: 10.1007/978-3-642-55315-8_1
3. Basile, F. et al. (2010) Combined Use of Synchrotron Radiation Based Imaging Techniques for the Characterization of Structured Catalysts, *Advanced Functional Materials*, 20, 4117–4126. doi: 10.1002/ADFM.201001004
4. Bergmann, U. et al. (2002a) Bulk-sensitive XAS characterization of light elements: From X-ray Raman scattering to X-ray Raman spectroscopy, *Microchemical Journal*, 71, 221–230. doi: 10.1016/S0026-265X(02)00014-0
5. Bergmann, U. et al. (2002b) X-ray Raman spectroscopy at the oxygen K edge of water and ice: Implications on local structure models, *Physical Review B*, 66, 092107. doi: 10.1103/PhysRevB.66.092107
6. Braun, A. et al. (2015) Hard X-rays in–soft X-rays out: An operando piggyback view deep into a charging lithium ion battery with X-ray Raman spectroscopy. *Journal of Electron Spectroscopy and Related Phenomena*, 200, 257-263. doi: 10.1016/j.elspec.2015.03.005
7. Brown, G.E. and Sturchio, N.C. (2002) An Overview of Synchrotron Radiation Applications to Low Temperature Geochemistry and Environmental Science, *Reviews in Mineralogy and Geochemistry*, 49 (1) , 1-115. doi: 10.2138/gsrmg.49.1.1
8. Cai Y. Q. et al. (2005) Ordering of hydrogen bonds in high-pressure low-temperature H₂O, *Physical Review Letters*, 94, 025502. doi: 10.1103/PhysRevLett.94.025502

9. Cotte, M. et al. (2010) Synchrotron-Based X-ray Absorption Spectroscopy for Art Conservation: Looking Back and Looking Forward, *Accounts of Chemical Research*, 43 (6),705–714. doi: 10.1021/ar900199m
10. Fukui, H. et al. (2007) Oxygen K-edge fine structures of water by x-ray Raman scattering spectroscopy under pressure conditions, *Journal of Chemical Physics*, 127, 134502. doi: 10.1063/1.2774988
11. Gomez, A. et al. (2018) The high-energy x-ray diffraction and scattering beamline at the Canadian Light Source, *Review of Scientific Instruments*, 89, 063301. doi: 10.1063/1.5017613
12. Gueriau, P. et al. (2017) Noninvasive Synchrotron-Based X-ray Raman Scattering Discriminates Carbonaceous Compounds in Ancient and Historical Materials. *Analytical Chemistry*, 89 (20), 10819-10826. doi: 10.1021/acs.analchem.7b02202
13. Hämäläinen, K. and Manninen, S. (2001) Resonant and non-resonant inelastic x-ray scattering, *Journal of Physics-Condensed Matter*, 13 (34), 7539–7555. doi: 10.1088/0953-8984/13/34/306
14. Huotari, S. et al. (2010) Direct tomography with chemical-bond contrast, *Nature Materials*, 10 (7), 489–493. doi: 10.1038/nmat3031
15. Iwamoto, H. (2018) Synchrotron Radiation X-ray Diffraction Techniques Applied to Insect Flight Muscle, *International Journal of Molecular Sciences*, 19 (6), 1748. doi: 10.3390/ijms19061748
16. Iitaka T. et al. (2015) Pressure-induced dissociation of water molecules in ice VII, *Scientific Reports*, 5, 12551. doi: 10.1038/srep12551
17. Jonas A. et al. (2014) Comparison of x-ray absorption spectra between water and ice: New ice data with low pre-edge absorption cross-section, *Journal of Chemical Physics*, 141, 034507. doi: 10.1063/1.4890035
18. Lee, S. K. et al. (2014) Probing of pressure-induced bonding transitions in crystalline and amorphous earth materials: insights from X-ray Raman scattering at high pressure, *Reviews in Mineralogy and Geochemistry*, 78 (1), 139-174. doi: 10.2138/rmg.2014.78.4
19. Lindegaard-Andersen, A. and Gerward, L. (1995) Röntgen centenary-100 years of X-rays, *Radiation Physics and Chemistry*, 46 (3), 299–302. doi: 10.1016/0969-806X(95)00063-4
20. Lutzenkirchen-Hecht, D. et al. (2014) The multi-purpose hard X-ray beamline BL10 at the DELTA storage ring, *Journal of Synchrotron Radiation*, 21, 819-826. doi: 10.1107/S1600577514006705
21. Mao W. L. et al. (2006) X-ray-induced dissociation of H₂O and formation of an H₂O₂ alloy at high pressure, *Science*, 314, 636–638. doi: 10.1126/science.1132884
22. McCarthy, A. A. et al. (2018) ID30B—a versatile beamline for macromolecular crystallography experiments at the ESRF, *Journal of Synchrotron Radiation*, 25, 1249–1260. doi: 10.1107/S1600577518007166
23. Moffat, K. and Ren, Z. (1997) Synchrotron radiation applications to macromolecular crystallography, *Current Opinion in Structural Biology*, 7 (5), 689-696. doi: 10.1016/S0959-440X(97)80079-6
24. Myneni, S. et al. (2002) Spectroscopic probing of local hydrogen-bonding structures in liquid water, *Journal of Physics Condensed Matter*, 14 (8), L213. doi: 10.1088/0953-8984/14/8/106

25. Näslund, L. Å. et al. (2005) X-ray absorption spectroscopy measurements of liquid water, *Journal of Physical Chemistry B*, 109 (28), 13835-13839. doi: 10.1021/jp052046q
26. Nilsson, A. et al. (2010) X-ray absorption spectroscopy and x-ray Raman scattering of water and ice: an experimental view, *Journal of Electron Spectroscopy and Related Phenomena*, 177 (2-3), 99–129. doi: 10.1016/j.elspec.2010.02.005
27. Parent, P. et al. (2002) Structure of the water ice surface studied by x-ray absorption spectroscopy at the O K-edge, *Journal of Chemical Physics*, 117, 10842–10851. doi: 10.1063/1.1519256
28. Richard, F. et al. (2001) *TESLA Technical Design Report Part I Executive Summary*, ISBN: 3-935702-00-0, ISSN: 0418-9833
29. Sahle C. J. et al. (2013) Microscopic structure of water at elevated pressures and temperatures, *Proceedings of the National Academy of Sciences*, 110, 6301–6306. doi: 10.1073/pnas.1220301110
30. Sahle, C. J. et al. (2015) Planning, performing and analyzing X-ray Raman scattering experiments, *Journal of Synchrotron Radiation*, 22, 400-409. doi: 10.1107/S1600577514027581
31. Sahle, C. J. et al. (2016). In situ characterization of the decomposition behavior of Mg (BH₄)₂ by X-ray Raman scattering spectroscopy. *Physical Chemistry Chemical Physics*, 18 (7), 5397-5403. doi: 10.1039/C5CP06571B
32. Smith, J. D. et al. (2006) Probing the local structure of liquid water by x-ray absorption spectroscopy, *Journal of Physical Chemistry B*, 110 (40), 20038–20045. doi: 10.1021/jp063661c
33. Tse, J. S. et al. (2008) X-ray Raman spectroscopic study of water in the condensed phases, *Physical Review Letters*, 100, 095502. doi: 10.1103/PhysRevLett.100.095502
34. Yano, J. and Yachandra, V. K. (2009) X-ray absorption spectroscopy, *Photosynthesis Research*, 102, 241–254. doi: 10.1007/s11120-009-9473-8

